

Journal of Tribology Science and Technology

Original Research Article
Publication Date: 24 October 2025
Submission Date: 29 June 2025

ANALYSIS OF POROUS SURFACE SECTORIAL RECESS HYDROSTATIC THRUST BEARING OPERATING WITH NON-NEWTONIAN LUBRICANT

Anil Verma¹, Vivek Kumar², Vinay Panwar³

- ¹⁻³ Department of Mechanical Engineering, Netaji Subhas University of Technology (NSUT), New Delhi - 110078, India.
- *Email: vivek.kumar@nsut.ac.in (Corresponding Author)

ABSTRACT

This article presents numerical simulations of a porous surface sectorial recess hydrostatic thrust bearing considering the shear-thinning behavior of a lubricant. The Rabinowitsch fluid model is used to describe the shear-thinning nature of the lubricant. Darcy's law was used to describe the flow of a lubricant through a porous surface. Three compensating elements namely capillary, orifice, and constant flow valves were used to supply lubricant to the bearing. A generalized form of the non-Newtonian Reynolds equation was solved using the finite element approach. The Newton-Raphson method is used to solve the global system of equations, obtain after finite element weak formulation. The perturbation technique was used to evaluate the rotor-dynamic parameter, stiffness, and damping parameters. Effects of the permeability of porous layer, flow coefficient of lubricant, and compensating elements are analyzed on the film pressure, load-carrying capacity, lubricant flow rate, stiffness, and damping parameters. It was found that the use of a porous layer and shear thinning of a lubricant adversely affect the abovementioned performance indices. The constant flow valve, as compared to the capillary and orifice compensators offers more load-carrying capacity, stiffness, and damping parameters. Therefore, a constant flow valve should be preferred in the hydrostatic thrust bearings to achieve better dynamic performance.

KEYWORDS: Hydrostatic Bearing, Sectorial Recess, Porous Surface, Shear-thinning lubricant, Compensating Elements.

1. INTRODUCTION

Hydrostatic thrust bearings are extensively used to support heavily loaded machines/structures operating at relatively low speed or even zero speed. These bearings offer excellent stiffness and damping characteristics [1], which are essential for highly precise and accurate machine motion. The operational performance of a hydrostatic bearing primarily depends on the selection of the compensating elements, lubricant, and configuration of the recess. Many researchers have investigated the use of non-conventional recess configurations such as annular [2-3], circular [4], elliptical pad [5], rectangular pad [6], etc., on the performance of hydrostatic thrust bearings. In addition, the influence of compensating elements on the steady-state operation of hydrostatic bearings was investigated. A capillary tube is mostly used as compensating element to

regulate the supply pressure of the lubricant and flow rate in the bearings. Numerical and experimental simulations have been reported with capillary [1, 6], control flow valve [7], orifice [1], membrane [4], porous surface in conjunction with capillary restrictor [6-7], displacement compensator [9], etc., used as a compensating element in hydrostatic thrust bearings. Hanawa et al. [6] conducted an experimental simulation to study the effect of providing a porous surface on the static stiffness of thrust bearings. The authors suggested a clearance range within which the porous land bearing would provide a better static stiffness than conventional porous and pocketed bearings. Recently, an investigation [9] reported that a displacement compensator would provide a high stability margin for an adaptive stepped hydrostatic thrust bearing.

Most commercially available lubricants exhibit shear-thinning

characteristics during the operation of fluid-film bearings. Many studies have been reported using different lubricant models, such as the micropolar model [9], couple-stress model [3], and Rabinowitsch model [2, 10], to simulate the flow of non-Newtonian lubricants in fluid-film bearings. Wada and Hayashi [11] performed experimental studies and observed the shear-thinning nature of the lubricant in a journal bearing. The authors found that the Rabinowitsch fluid model closely approximates the pseudoplastic nature of lubricants. Wu and Dareing [12] theoretically and experimentally investigated a control-flow-valve compensated thrust bearing lubricated with an ethylene glycol-based oil blended with traces of graphite powder. The authors used the power law to model the shearthinning behavior of the lubricant in the analytical analysis. Singh et al. [2, 10] performed a numerical simulation of a hydrostatic thrust bearing considering the inertia effects and shear-thinning nature of the lubricant. The lubricant was numerically modelled using the Rabinowitsch fluid model. Theoretical and experimental studies [13-14] have been conducted to study the effects of long-chain polymer additives on the load-carrying capacity and friction coefficient of sliding surfaces. The viscoelastic Maxwell model, finitely extensible nonlinear elastic (FENE) model and couple-stress model [13] were compared in terms of load-carrying capacity in hydrodynamic lubrication. The Maxwell and FENE models were found to reduce the load-carrying capacity, whereas the couple-stress model was found to enhance the load-carrying capacity. Experimental studies [14] have been reported on the rheology of SAE 30 engine oil blended with TiO₂ nanoparticles with different volume fractions. With advancements in manufacturing techniques, researchers and bearing designers are exploring the usefulness of non-conventional recess shapes such as annular, circular, and elliptical to enhance the performance of thrust bearings. Advanced manufacturing techniques [15-17] such as micromachining, stereolithography, laser surface texturing, etc., can modify the bearing geometry

2. MATHEMATICAL MODEL

The schematic/layout of the hydrostatic thrust bearing considered for the investigation is depicted in figure 1. A lubricant was supplied to the bearing through compensating elements. A porous layer is applied to the land region of the thrust pad. A sectorial recess with four sectors is provided in the thrust pad. Unlike hydrodynamic bearings, these bearings can support and lift the runner even at very low or zero speeds, such as in telescopes, observatory domes, hydrostatic lift in stadiums and antenna systems. As illustrated in Figure 1, the bearing and runner surfaces remain parallel, and no physical wedge is formed between runner and bearing surfaces. Consequently, velocity or wedge-effect terms are not considered in the present analysis. The flow of a non-Newtonian lubricant on the porous surface of the thrust pad is expressed using the modified non-dimensional form of the Reynolds equation.

dimensional form of the Reynolds equation,

$$\frac{\partial}{\partial \bar{x}} \left(\bar{F}_2 \{ \bar{h}^3 + \psi \} \frac{\partial \bar{p}}{\partial \bar{x}} \right) + \frac{\partial}{\partial \bar{y}} \left(\bar{F}_2 \{ \bar{h}^3 + \psi \} \frac{\partial \bar{p}}{\partial \bar{y}} \right) = \frac{\partial \bar{h}}{\partial \bar{t}}$$
(1)

even at the microscale. It has been reported that incorporating micro-patterns of different shapes and configurations [18-19] on the bearing surface can significantly improve the load-carrying capacity and reduce the frictional power loss in thrust bearings.

Thrust bearings with porous layers are commercially economical and require less space than conventional impermeable surfaces. Lubricant flow in porous layers is generally described using the Darcy model. Some investigations have been performed to compare the operation of porous surface bearings to that of impermeable surface bearings. These investigations [20-24] examined the influence of the permeability of the porous layer on the load-carrying ability and coefficient of friction. It was reported that an increase in the permeability of the porous facing slightly reduced the load-carrying ability and increased the coefficient of friction. Surface roughness (to a certain degree) is inherent to all machining processes. When the magnitude of the surface roughness is of the order of the film thickness, it is essential to consider the topography of the bearing surface in the analysis. Patir and Cheng [25] proposed a roughness model based on the average film thickness between rough bearing surfaces. The proposed model incorporates pressure and shear flow factors into the generalized Reynolds equation. Investigations [26-27] have been conducted to study the effect of the surface roughness on the load-carrying capacity and squeeze time of parallel plates. The authors reported that the surface roughness tends to enhance the load-carrying capacity and squeeze time of plates. After reviewing the available literature, it was noticed that there exists a research gap and scope to carry out a comprehensive investigation on the influence of the permeability of the porous layer, compensating elements, and shear thinning of the lubricant for steady-state and the dynamic response of sectorial recess hydrostatic thrust bearings.

where \bar{F}_2 is the cross-viscosity integral and ψ is the permeability parameter. The squeeze velocity $\left(\frac{\partial \bar{h}}{\partial \bar{t}}\right)$ of the runner surface is defined as the rate of change of the film thickness with time. The squeeze velocity at the pad surface is described by Darcy's Law and the continuity equation. The velocity of the fluid in the porous layer is given by:

$$u_n = -\frac{k}{\mu} \frac{\partial P}{\partial n} \tag{2}$$

The shear-thinning nature of the fluid is expressed using the Rabinowitsch fluid model.

$$\bar{\tau} + k\bar{\tau}^3 = \bar{\gamma} \tag{3}$$

where k is the flow index of a non-Newtonian lubricant. The numerical value of k=0 describes Newtonian lubricant, and k=0.58 describes a pseudoplastic lubricant.

The numerical simulation of Equation 1 was performed using the finite-element numerical technique. The land region of the pad is divided into sub-areas by 4-node quadrilateral elements. The lubricant pressure was assumed to vary linearly along the length and width of these elements.

$$\bar{p} = \sum_{i=1}^{4} [N_i \overline{p}_i]; \ N_j = \frac{1}{4} (1 + \xi_i \xi) (1 + \eta_i \eta)$$
 (4)

The multi-sectorial recess discretization consists of 933x864,

nodes and elements. The grid size was obtained following the grid independence test. Applying Galerkin's weighted residual approach to Equation 1 yields

$$\iint N_{i} \left(\frac{\partial}{\partial \bar{x}} \left(\left\{ \bar{h}^{3} + \psi \right\} \frac{\partial}{\partial \bar{x}} \left\{ \sum_{i=1}^{4} (\bar{p}_{i} N_{i}) \right\} \right) + \frac{\partial}{\partial \bar{y}} \left(\left\{ \bar{h}^{3} + \psi \right\} \frac{\partial}{\partial \bar{y}} \left\{ \sum_{i=1}^{4} (\bar{p}_{i} N_{i}) \right\} \right) - \frac{\partial \bar{h}}{\partial \bar{t}} \right) d\bar{x} d\bar{y} = 0$$
(5)

The simplification of the above equation leads to,

$$\left[\bar{F}_{ij}^{e}\right]\left\{\bar{p}\right\} = \left[\bar{Q}_{i}^{e}\right] + \bar{h}\left[\overline{RS}_{i}^{e}\right] \tag{6}$$

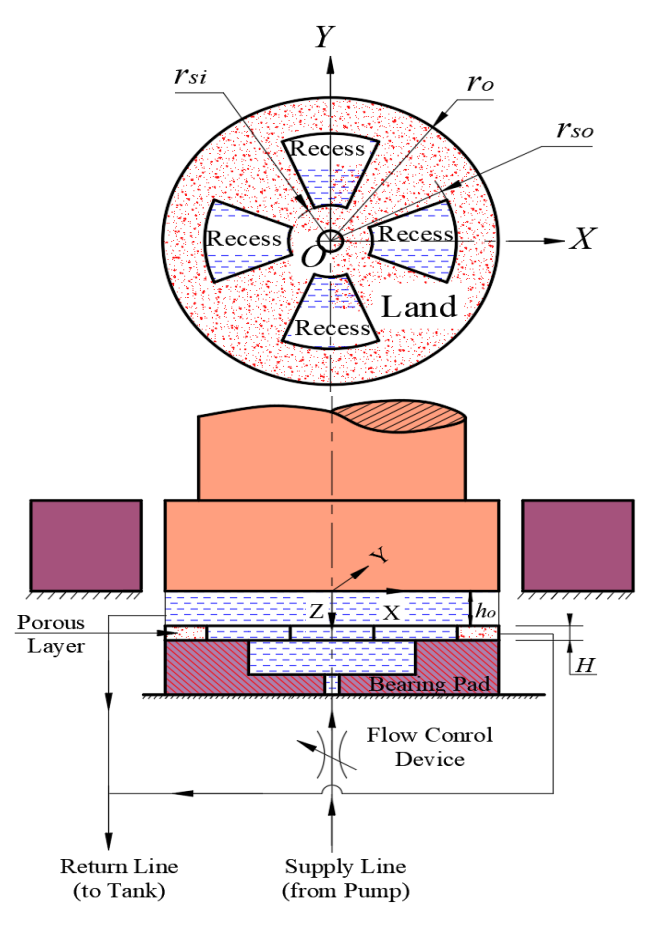


Fig. 1. Hydrostatic Thrust Bearing with Porous Surface and Sectorial Recess Design

The nodes lying on the thrust pad outer boundary (R_o) were allocated atmospheric pressure values. The lubricant is fed to sectorial recess by considering various types of compensating elements (capillary n=1, orifice n=0.5, and constant-flow valve n=0). Subsequently, the fluid flow rate through the compensating elements must be coupled with the fluid flow rate from the bearing. To do so, the algebraic sum of the flow rate

via nodes present on recess boundaries is set equal to the flow rate via compensating elements (Figure 2). This will ensures that the lubricant input flow rate is equal to the lubricant flow rate through restrictor or lubricant leakage rate at the outer boundary of thrust pad.

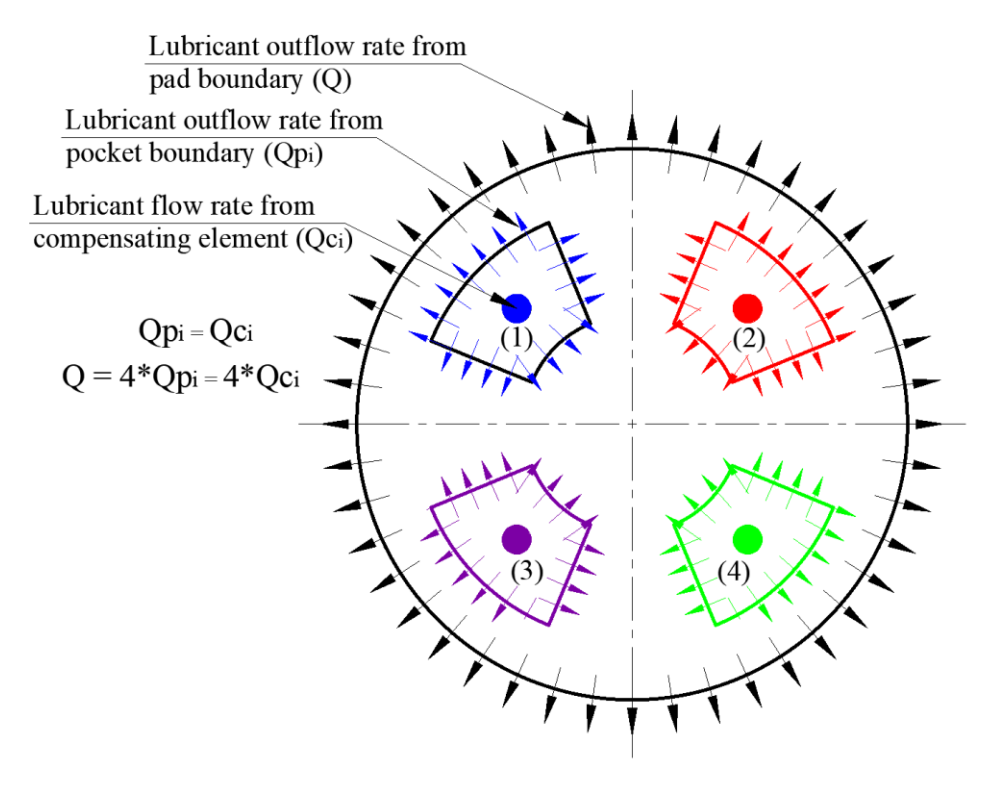


Figure 2: Schematic for balancing of lubricant flow rate through compensating element and bearing

$$\begin{bmatrix} \bar{F}_{11} & \bar{F}_{12} & \dots & \bar{F}_{1j} & \dots & \bar{F}_{1n} \\ \bar{F}_{21} & \bar{F}_{22} & \dots & \bar{F}_{2j} & \dots & \bar{F}_{2n} \\ \vdots & \vdots & \vdots & \vdots & \vdots & \vdots \\ \bar{F}_{j1} & \bar{F}_{j2} & \dots & \bar{F}_{jj} & \dots & \bar{F}_{jn} \\ \vdots & \vdots & \vdots & \vdots & \vdots & \vdots \\ \bar{p}_{o} & \vdots & \vdots & \vdots & \vdots \\ \bar{p}_{on} \end{bmatrix} = \begin{bmatrix} \bar{q}_{1} \\ \bar{q}_{2} \\ \vdots \\ \bar{q}_{comp} = C_{comp} (1 - \bar{p}_{o})^{n} \\ \vdots \\ \bar{q}_{n} \end{bmatrix} + \bar{h} \begin{bmatrix} \bar{r}\bar{s}_{1} \\ \bar{r}\bar{s}_{2} \\ \vdots \\ \bar{r}\bar{s}_{j} \\ \vdots \\ \bar{r}\bar{s}_{n} \end{bmatrix}$$

$$(7)$$

The Newton Raphson method was used to solve the above Equation (7), to compute steady-state $(\bar{h}=0)$ film pressure distribution (p) on the thrust pad. The nodal pressures were integrated on the pad surface to compute the non-dimensional load-carrying capacity (\bar{W}) and lubricant flow rate (\bar{q}) . In the present work, Equation (7) was first solved under steady-state conditions $(\bar{h}=0)$ to obtain the converged solution of the bearing system. The resulting fluid-film pressure values were then integrated over the bearing domains to evaluate the load carrying capacity (\bar{W}) . Subsequently, a perturbation was

introduced in the film thickness $(\Delta \bar{h} = 10^{-04})$ and the source code was executed for a single iteration to compute the fluid film pressure and pressure gradient. The corresponding pressure distribution obtained from the simulation was again integrated over the bearing domains to yield the stiffness coefficients as outlined by Equation (9). Similarly, the damping coefficients were evaluated by perturbing the runner's normal velocity $(\Delta \bar{h} = 10^{-04})$ in accordance with Equation (10). Pressure gradients were integrated over the pad surface to compute the non-dimensional stiffness (K), and damping (D) parameters.

Load-carrying capacity:
$$\overline{W} = \sum_{e=1}^{4} \left\{ \int_{-1}^{+1} \int_{-1}^{+1} \left(\sum_{j=1}^{4} \bar{p}_{i} N_{i} \right) |\bar{J}| d\xi d\eta \right\} + \sum_{e=1}^{n_{p}} \bar{A}_{p} \bar{p}_{r}$$
 (8)

Stiffness parameter:
$$\bar{K} = \sum_{e=1}^{4} \left\{ \int_{-1}^{+1} \int_{-1}^{+1} \left(\sum_{i=1}^{4} \frac{\partial \bar{p}_{i}}{\partial \bar{h}} N_{i} \right) |\bar{J}| d\xi d\eta \right\} + \sum_{e=1}^{n_{p}} \bar{A}_{p} \frac{\partial \bar{p}_{r}}{\partial \bar{h}}$$
 (9)

Damping parameter:
$$\bar{C} = \sum_{e=1}^{4} \left\{ \int_{-1}^{+1} \int_{-1}^{+1} \left(\sum_{i=1}^{4} \frac{\partial \bar{p}_{i}}{a\bar{k}} N_{i} \right) |\bar{J}| d\xi d\eta \right\} + \sum_{e=1}^{n_{p}} \bar{A}_{p} \frac{\partial \bar{p}_{r}}{a\bar{k}}$$
 (10)

3. SOLUTION METHODOLOGY

The numerical simulations of the bearing were achieved via a finite element weak formulation of the modified Reynold's equation (1). The effect of the porosity of porous layer of thrust pad, shear-thinning behavior of lubricant, and compensating elements is incorporated through various laws and equations as described in the preceding section. An iterative source code utilizing the finite element formulation and solution of the Reynolds equation by the Newton-Raphson method was developed to simulate the bearing numerically. The dimensional and operating parameters used to study bearing are provided in table 1 [6, 23-24]. The sectorial recessed pad surface was discretized using 4 node quad elements. The number of nodes and elements used in the discretization of the pad surface were 933 and 864, respectively. The steps in the algorithm (Figure 3) used to perform the numerical simulations of the bearing are as follows,

- 1. Input bearing geometry and operating parameters.
- Meshing of the pad using 4 node quad elements. Initialize parameters, such as viscosity, viscosity

- integrals, shear stress, strain rate, voltage, film pressure, and pressure gradients.
- 3. Establish gauss points and weights for elements. Initialize the value of fluid-film thickness.
- 4. Perform finite element formulation of the Reynolds equation, Continuous Bingham model, and compensating element fluid flow equation (Eqs. 1-5).
- 5. Assembly of the weak form of Reynolds equation (Eq.6).
- 6. Solve Reynolds equation using Newton Raphson method for film pressure (Eq.7).
- 7. Check the convergence of the film pressure values. If the condition is satisfied, proceed to step 8, otherwise move back to step 3.
- 8. Compute lubricant flow rate and load-carrying capacity (Eq.8)
- 9. Use perturbation concerning the film thickness and squeeze velocity to compute the stiffness and damping parameters (Eqs. 9-10).

Table 1: Dimensional and operating parameter of bearing

Parameter	Value
Radius of pad (R_o)	100 mm
Sectorial recess dimension	$R_{so} = 75 \text{ mm}; R_{si} = 25 \text{ mm}$
Reference film thickness	50 μm
Supply pressure	1 MPa
Viscosity of lubricant	34 mPa.s
Permeability parameter	0, 0.05
Lubricant flow index	0, 0.58

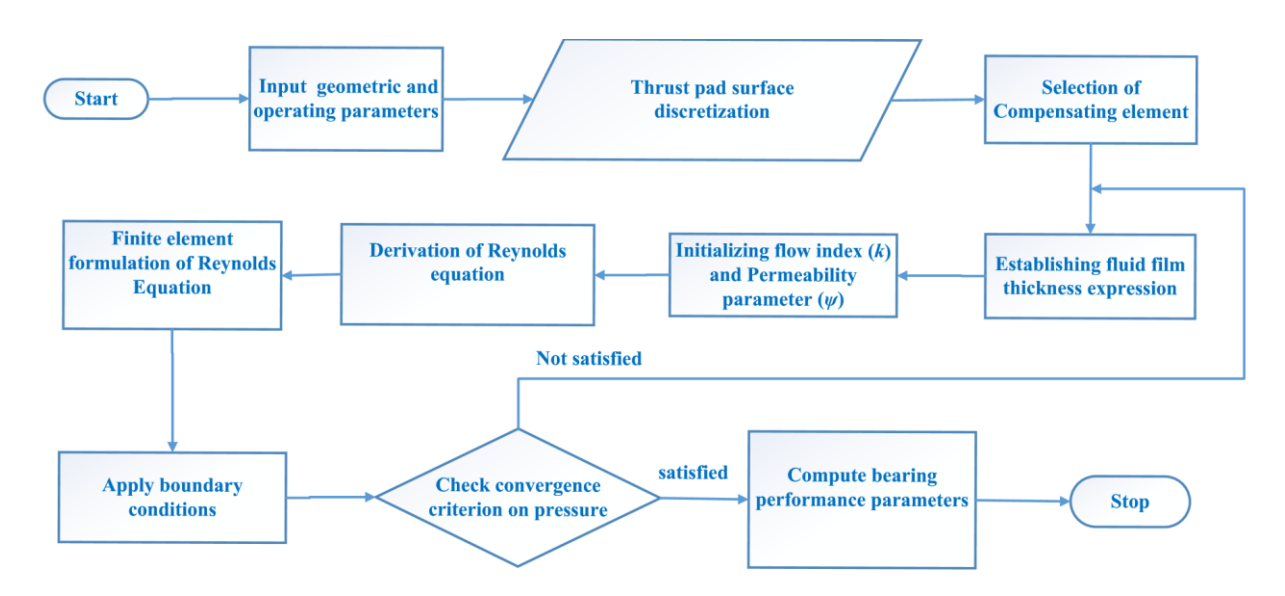


Fig. 3. Solution Scheme

The iterative solution algorithm was assumed to be converged, once a convergence of 10^{-06} was achieved on film pressure values between the successive iterations. After achieving the convergence, the load-carrying capacity, stiffness, and damping parameters were computed from the film pressure values as described in the preceding section. Before computing the numerical results, the solution algorithm (discussed above) was validated using a reference study [6]. The authors of the reference study have conducted numerical/experimental simulations for a rectangular hydrostatic thrust bearing. A

porous facing was provided over the land area of the pad. The water (lubricant) was fed to the rectangular recess via a capillary tube. The source code from the present study is used to regenerate the results of the reference study. A comparison of the numerical and experimental results between the reference study and the developed mathematical model is shown in Figure 4. A maximum difference of -5.5 % was observed in the numerical results. This difference can be attributed to the solution scheme (FEM versus FDM), convergence criteria, and grid size adopted in the two studies.

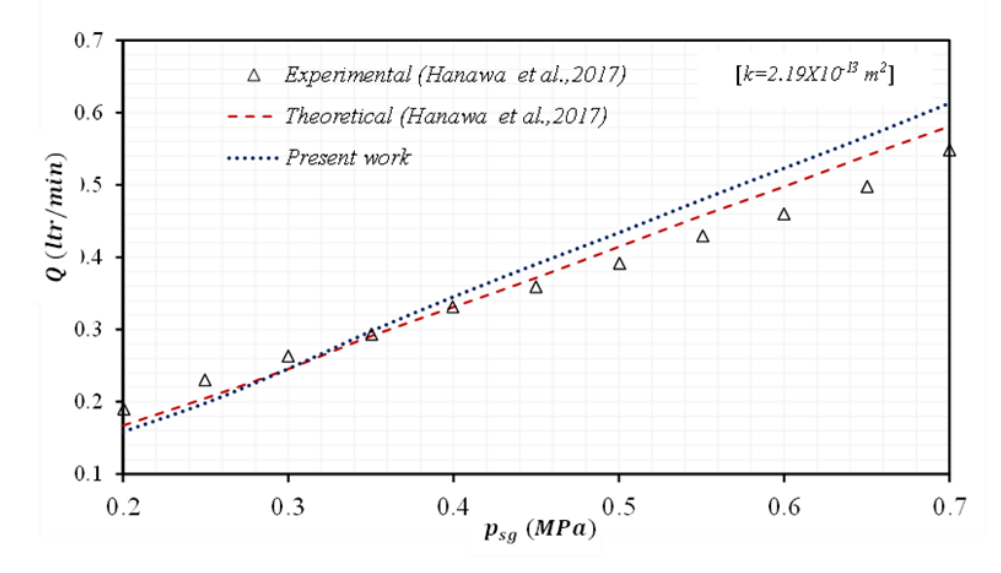


Fig. 4. Lubricant supply pressure (p_{sg}) versus lubricant flow rate (Q).

4. RESULTS AND DISCUSSIONS

In this section, the numerical results for a porous surface sectorial recess thrust bearing employing a non-Newtonian lubricant are discussed. The influence of porosity, shear-thinning of the lubricant, and compensating elements are discussed on the non-dimensional film pressure (\bar{p}) , load-carrying capacity (\bar{W}) , flow rate (\bar{q}) , stiffness (\bar{K}) , and damping (\bar{C}) parameters. The bearing geometric and operating parameters were used from the available literature. Two values of the permeability parameter (ψ) were used to numerically treat the impermeable $(\psi=0)$ and the porous $(\psi=0.05)$ surfaces. Similarly, the linear and non-linear nature of the lubricant is considered by assigning values of θ and θ .58 to the lubricant flow index (k). For comparison, impermeable surface sectorial recess capillary-compensated thrust bearing operating with a Newtonian lubricant was treated as a base bearing.

Figure 5 illustrates the effects of the permeability parameter (ψ) and flow index (k) on the film pressure profile for a sectorial recess thrust bearing. It is visible that the shear-thinning of the lubricant (k=0.58) adversely affected the film pressure. When a non-Newtonian lubricant with shear-thinning characteristics is used, its viscosity decreases with increasing shear rate. In

hydrostatic thrust bearings, where the lubricant film is pressurized externally and subjected to shear due to relative surface motion, this reduction in viscosity lowers the resistance to flow within the film. As a result, the pressure distribution within the film generally decreases compared to that with a Newtonian lubricant of constant viscosity. In addition, the use of a porous layer (ψ =0.05) also reduces the pressure values. The introduction of a porous layer in a hydrostatic thrust bearing significantly alters the film pressure profile. The porous matrix allows part of the pressurized lubricant to seep through its interconnected pores, leading to a reduction in the effective film pressure within the clearance space. This pressure drop generally lowers the peak pressure and smoothens the pressure distribution across the bearing surface. Figure 6 shows the effect of film thickness on the recessed pressure (\bar{p}_r) . It was found that the recess pressure decreased with a gradual increase in film thickness. The bearing with a porous layer and shearthinning of the lubricant generated lower values of pressure in the recess. This reduction in pocket pressure is noticed in the range of -2.1 % to -13.5%. A higher reduction in pocket pressure was noticed at the low value of film thickness.

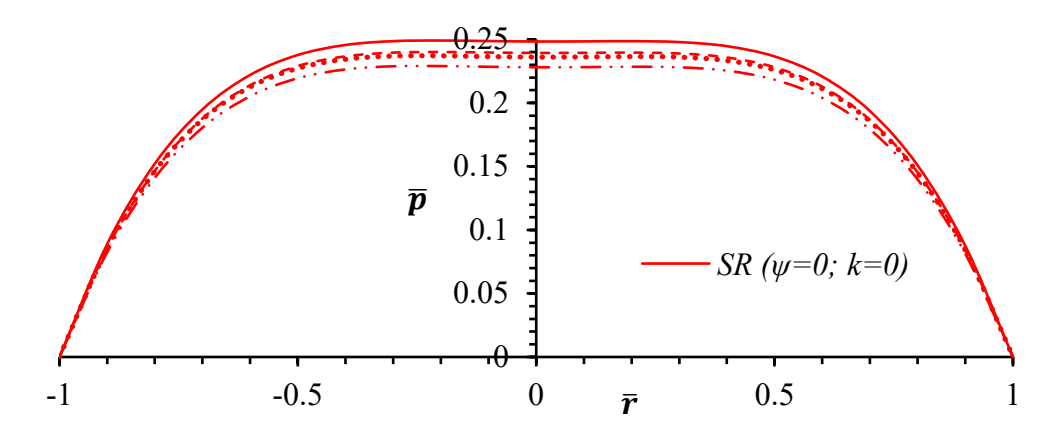
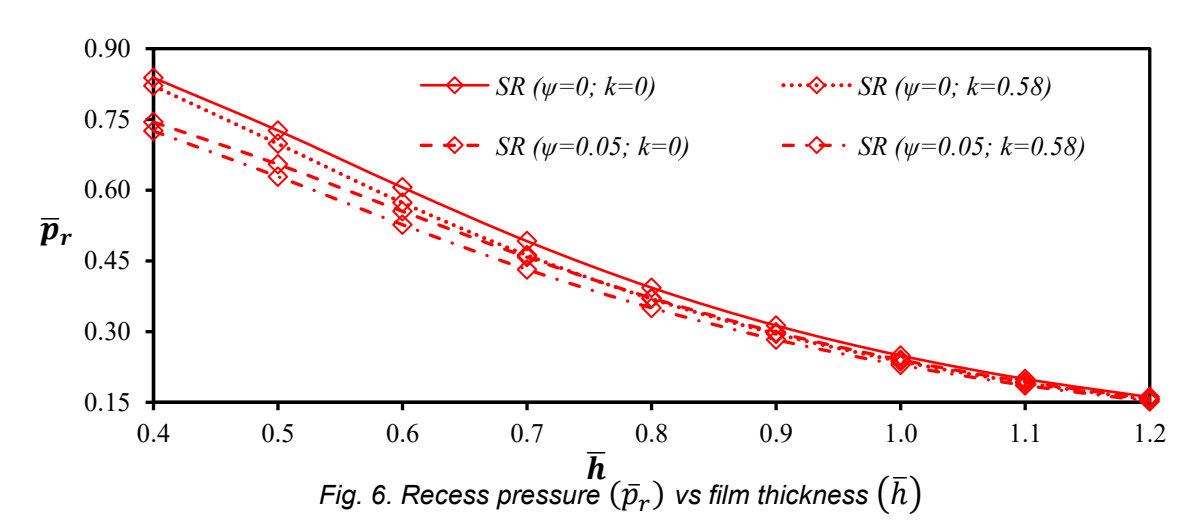


Fig. 5. Film Pressure (\bar{p}) profile along x-axis (diametrical line: \bar{r})



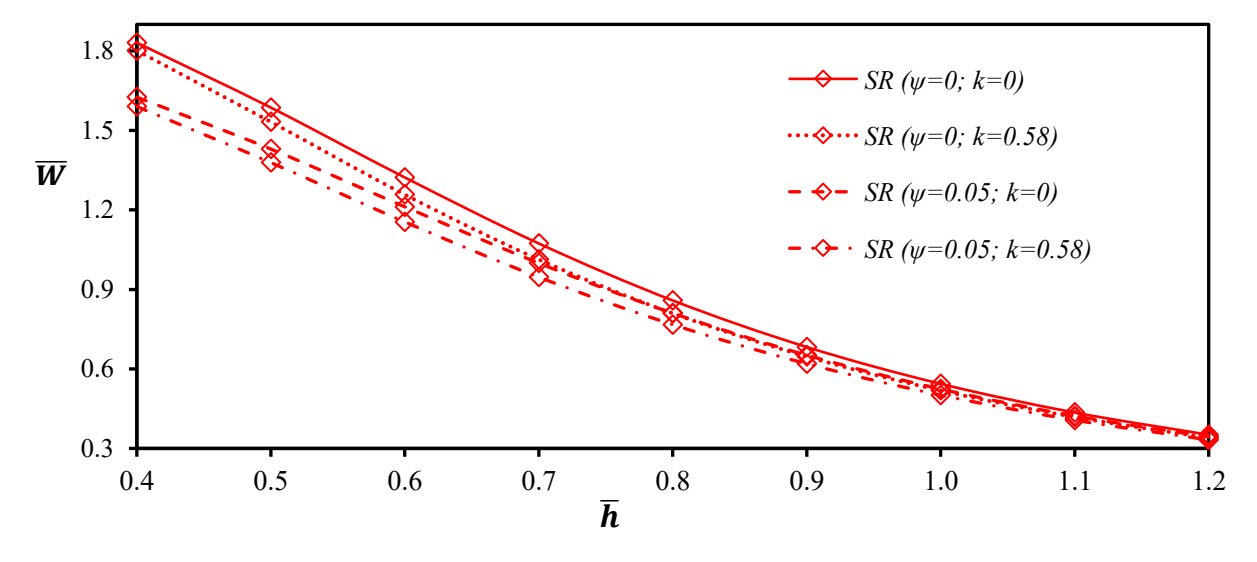


Fig. 7. Load-carrying capacity (\overline{W}) vs film thickness (\overline{h})

T 11 0 1 0	•			•	
Lania 'J' Infliianca	ot companeating	a alamant an	naarına	nartarmanca	INGICAC
Table 2: Influence	UI CUITIDETISALITI	u	Dealliu	Dellulliance	IIIUICES

Steady State Performance Parameters										
Compensating	$\overline{oldsymbol{arrho}}$			\overline{W}						
Element	k=0; $\psi=0$	k=0.58; $\psi=0$	$k=0; \psi = 0.05$	k=0.58; $\psi = 0.05$	$k=0; \psi$ =0	k=0.58; $\psi=0$	$k=0; \psi = 0.05$	k=0.58; $\psi = 0.05$		
CAP	0.7511	0.7633	0.7601	0.7713	0.5437	0.5185	0.5240	0.5010		
$\frac{(ORF - CAP)}{ORF} 100$	12.89	12.51	12.43	12.06	12.89	10.95	12.43	10.65		
$\frac{ORF}{(CFV - CAP)} 100$	33.13	31.01	31.55	29.66	33.13	26.43	31.55	25.55		
Dynamic Performance Parameters										
Compensating	\overline{K}			$\overline{\it c}$						
Element	k=0; $\psi=0$	k=0.58; $\psi=0$	$k=0; \psi = 0.05$	k=0.58; $\psi = 0.05$	$k=0; \psi$ =0	k=0.58; $\psi=0$	$k=0; \psi = 0.05$	k=0.58; $\psi = 0.05$		
CAP	1.2236	1.1298	1.1367	1.0546	1.8407	1.6358	1.7705	1.5830		
$\frac{(ORF - CAP)}{ORF} 100$	25.70	20.83	24.83	20.35	9.44	5.21	9.19	5.27		
$\frac{(CFV - CAP)}{CAP} 100$	77.11	55.61	72.95	53.86	27.52	13.10	26.26	13.18		

Figure 7 depicts the numerical results for the variation in the load-carrying capacity (\overline{W}) . It can seem that the porosity and fluid flow index have a negative effect on the load-carrying capacity. This is because of the lesser magnitude of film pressure generated on the recess and land area (Figure 5-6) in the presence of a porous layer and shear-thinning of the lubricant. The load carrying capacity of a hydrostatic thrust bearing is strongly influenced by both the rheological behavior of the lubricant and the use of a porous layer. When a shearthinning lubricant is employed, its viscosity decreases with increasing shear rate. This reduction in effective viscosity lowers the developed film pressure, thereby reducing the load carrying capacity compared to a Newtonian lubricant. Similarly, the presence of a porous layer allows part of the pressurized lubricant to leak through the pores, which diminishes the net pressure in the film region and consequently decreases the bearing's ability to sustain load. The synergistic effect of porosity and shear thinning reduces the load-carrying capacity up to -13.2% as compared to the base configuration of bearing. The numerical results presented in Table 2, show the effect of the compensating elements on the load-carrying capacity, lubricant flow rate, stiffness, and damping parameters of the sectorial recess bearing. The numerical results are presented only for sectorial recess capillary (CAP) compensated thrust bearing (base bearing). The enhancements in bearing performance indices were illustrated for the orifice (ORF) and constant flow valve (CFV) compensated bearings. It can be observed from the table that maximum load-carrying capacity (25.6% - 33.6%) was obtained using a constant flow valve followed by an orifice (10.9% - 12.9%) in the bearing system.

The numerical results for the lubricant flow rate (\bar{q}) are shown in Figure 8. It was observed that the shear-thinning nature of the lubricant enhanced the flow rate in the bearing. This could be due to the abatement in the viscosity of the lubricant because of the shear-thinning character of the lubricant. The slippage of the lubricant through the pores of the porous layer further enhanced the lubricant flow rate. Therefore, the presence of capillary-type pores in the thrust pad also favours a higher lubricant flow rate. The lubricant flow rate in a hydrostatic thrust bearing is affected by both shear-thinning behavior and the use of a porous layer. For a shear-thinning lubricant, the effective viscosity decreases with increasing shear rate, which reduces the flow resistance within the bearing clearance. As a result, the lubricant flow rate increases compared to that of a Newtonian lubricant under the same supply pressure. In the case of a porous layer, part of the lubricant seeps through the porous matrix, creating additional leakage paths. This also increases the overall flow rate demanded from the supply system to maintain the same film thickness and pressure level. Thus, while both shear-thinning and porosity lead to higher lubricant consumption, they influence the flow mechanism differently—shear thinning by reducing viscosity-dependent resistance, and porosity by providing alternate leakage channels. The combined effect of shear-thinning and porous layer enhanced the flow rate up to +69.8%. This enhancement in the lubricant flow rate was noticed to be profound at lower values of film thickness. The effect of the compensating elements on the lubricant flow rate under different operating conditions is presented in Table 2. It was found that constant flow valve and orifice compensation require a higher lubricant flow rate than capillary compensation for a given film thickness. Therefore, the pumping power requirement for capillary compensation is less than that of other methods of compensation in a bearing.

The effects of porosity and the pseudoplastic nature of the lubricant on the stiffness parameter of the bearing are illustrated in Figure 9. The stiffness characteristics of the bearing depend on the film pressure and pressure gradient values across the recess and land regions. The presence of a porous surface and shear-thinning of the lubricants reduce the film pressure value for a given film thickness. The stiffness characteristics of a hydrostatic thrust bearing depend on the ability of the lubricant film to resist deformation under applied load. When a shear-

thinning lubricant is used, the effective viscosity decreases with shear rate, leading to lower film pressure buildup. This reduction in film pressure weakens the bearing's load-deflection response, thereby decreasing the direct stiffness of the system. Similarly, incorporating a porous layer allows part of the supply lubricant to leak through the pores, which reduces the effective pressure in the film region. A significant drop (-16.7%) has been observed in the stiffness parameters because of the use of porous facing and shear thinning of lubricant. It was reported that the stiffness is maximum in a particular range of film thickness (0.5-0.6).

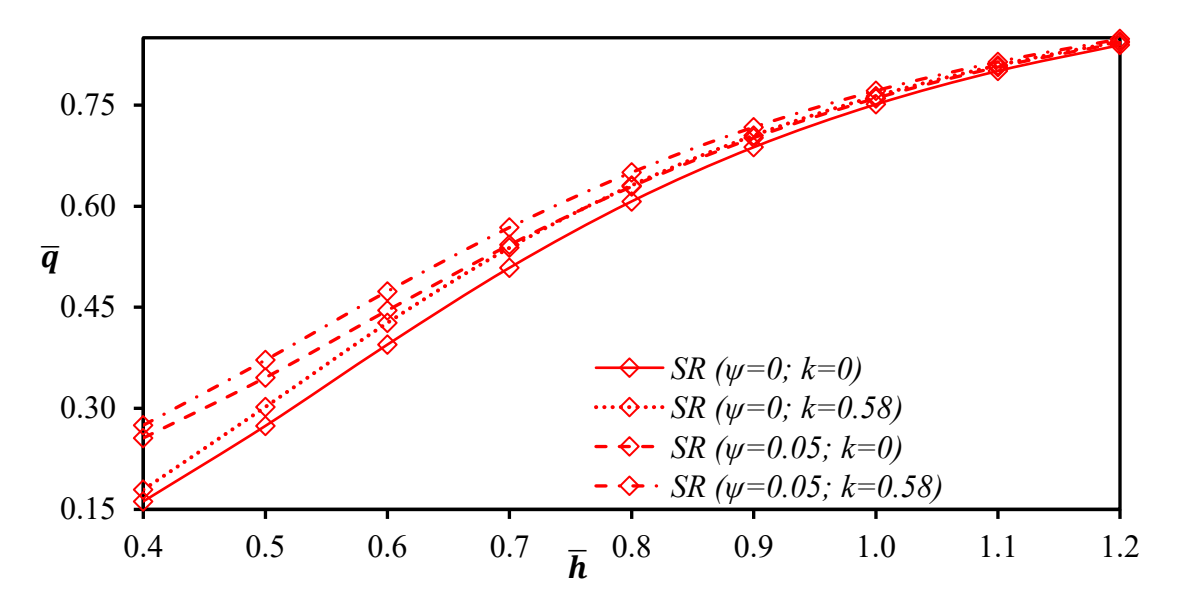


Fig. 8. Flow rate (\bar{q}) vs film thickness (\bar{h})

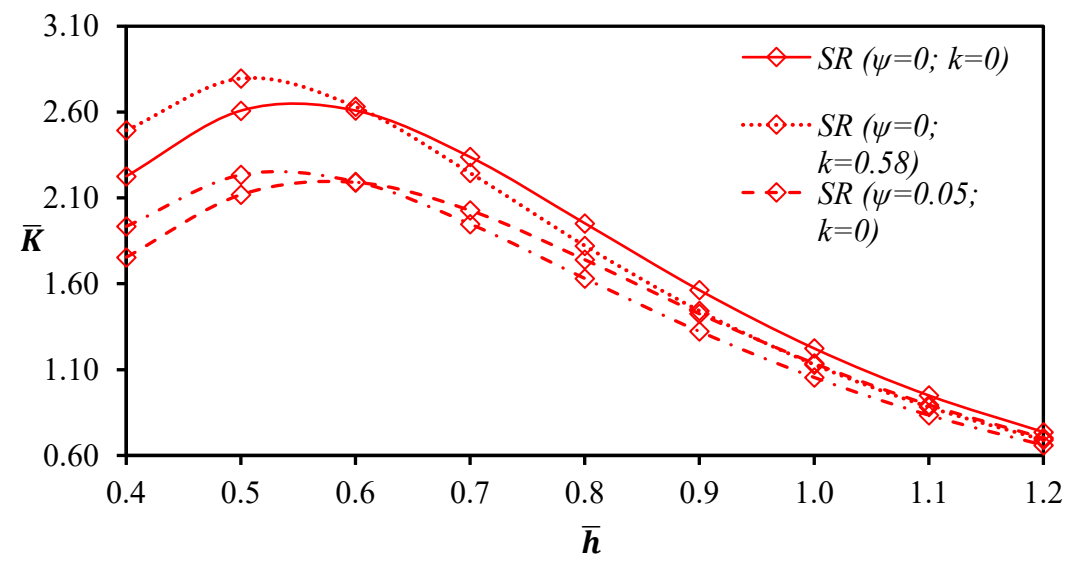


Fig. 9. Stiffness parameter (\overline{K}) vs film thickness (\overline{h})

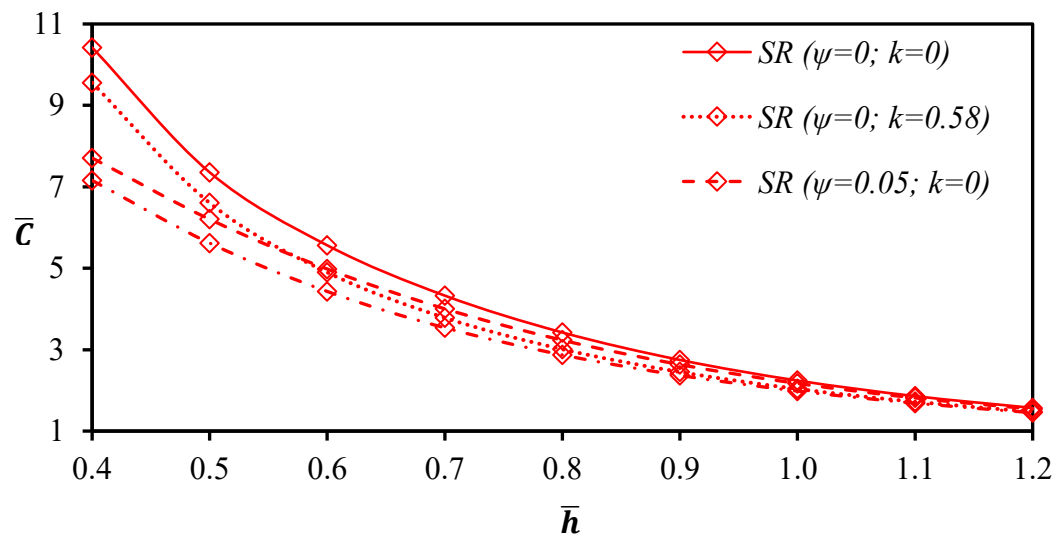


Fig. 10. Damping parameter (\bar{C}) vs film thickness (\bar{h})

In addition, the effect of the porous layer vis-à-vis the shearthinning of the lubricant is more domain in the reduction of the stiffness parameter. Hydrostatic thrust bearings are generally designed to operate at a specific film thickness, where the system achieves maximum stiffness [6]. For this reason, the maximum film stiffness values have been reported within the film thickness range of 0.5 to 0.6 (25 µm to 30 µm). The numerical results for the stiffness parameter presented in Table 2, suggest the use of a constant-flow-valve to improve the stiffness characteristics of the bearing. Figure 10 depicts the influence of the porosity and shear-thinning on the bearing damping parameter. The damping parameter was significantly reduced significantly with an increase in the film thickness. In addition, the porosity of the layer and the shear-thinning of the lubricant adversely affect the damping parameter. The damping characteristics of a hydrostatic thrust bearing are governed by the squeeze-film action and energy dissipation in the lubricant film. When a shear-thinning lubricant is used, its effective viscosity decreases with shear rate, which reduces the viscous resistance within the film. As a result, the damping coefficient decreases compared to that obtained with a Newtonian lubricant. In contrast, the use of a porous layer allows part of the pressurized lubricant to leak through the porous matrix. reducing the film pressure and altering the flow dynamics. This leakage diminishes the fluid film's ability to resist rapid squeeze motions, thereby lowering the damping capability of the bearing. The combined effect of porous facing and shear thinning of lubricant have reduced the damping parameter by the range of -2.4% to -32.5 %. Again, this effect is observed to be profound at of film thickness. A comparison of the various compensating elements in terms of the damping parameter is presented in Table 2. Under all operating conditions, the constant flow valve and orifice compensation offered a higher damping parameter valve. So, a constant flow valve is preferred

to achieve a better rotor dynamic response from the hydrostatic thrust bearing.

5. Conclusions

Numerical simulations of the sectorial recess hydrostatic thrust bearing were performed. The effects of the porosity of the thrust pad, shear-thinning of the lubricant, and compensating elements on the steady-state and rotor-dynamic performance are investigated. The use of a porous layer significantly reduced the pressure in the recess and land regions. Due to this, a loss of -11.2% was reported in the load-carrying capacity of bearing. The stiffness and damping parameters were also reduced by -21.2% and -27.1% respectively, due to the use of a porous layer. The shear-thinning of the lubricant also adversely affected the load-carrying capacity (-5.7%), stiffness (-7.7%), and damping (-13.8%) parameters. The influence of shear-thinning of the lubricant and porous layer on load-carrying capacity, stiffness, and damping parameters is profound at the low film thicknesses. In addition, a range of film thickness (0.5 -0.6) was found at which the stiffness parameter of the bearing achieved its maximum. The shear-thinning of the lubricant, use of a porous layer also enhances (+69.8%) the lubricant flow rate. This can enhance the pumping power of the bearings. The use of capillary compensation, compared to other compensation devices, effectively reduces the lubricant flow rate through the bearing. In practical terms, this implies that when capillaries are employed, the hydraulic resistance they introduce lowers the overall flow demand, thereby allowing the system to operate with a pump of lower power rating. This advantage of capillary compensation—enhancing energy efficiency by reducing pumping power requirements. Constant valve flow compensation as Compared to capillary and orifice compensation, provides a higher load-carrying capacity and better rotor-dynamic response from hydrostatic thrust bearings.

References

- [1] Harnoy, A., Bearing Design in Machinery: Engineering Tribology and Lubrication. CRC Press, 2002.
- [2] Singh, U. P., Gupta, R. S., And Kapur, V. K., "On The Application of Rabinowitsch Fluid Model on an Annular Ring Hydrostatic Thrust Bearing,". Tribology International, 58,2013, 65-70.
- [3] Kumar, V. And Sharma S. C., "Study of Annular Recess Hydrostatic Tilted Thrust Pad Bearing Under Influence of Couple Stress Lubricant Behaviour," International Journal of Surface Science and Engineering, 11, 2017, 344-369.
- [4] Chen, D. C., Chen, M. F., Pan, C. H. And Pan, J. Y., "Study of Membrane Restrictors in Hydrostatic Bearing," Advances in Mechanical Engineering, 10, 9, 2018, 1-8.
- [5] Maher, B. M, "Performance Characteristics of an Elliptic Hydrostatic Bearing and Comparative Analysis Based on Stokes' Conditions," Acta Mechanica, 223, 6, 2012,1187-98.
- [6] Hanawa, N., Kuniyoshi, M., Miyatake, M., And Yoshimoto, S., "Static Characteristics of a Water-Lubricated Hydrostatic Thrust Bearing with a Porous Land Region and a Capillary Restrictor," Precision Engineering, 50, 2017, 293-307.
- [7] Kumar, V., Shah, V. A., Singh, S. J., Narwat, K., And Sharma, S. C., "Rotor-dynamic performance of porous hydrostatic thrust bearing operating under magnetic field," Industrial Lubrication and Tribology, 73,1, 2021, 350-357.
- [8] Kumar, V., Sharma, S. C., And Narwat, K., "Analysis of control flow valve compensated thrust bearing considering thrust pad flexibility," Jurnal Tribologi, 25, 2021, 45-58.
- [9] Kodnyanko, V., Kurzakov, A., Grigorieva, O., Brungardt, M., Belyakova, S., Gogol, L., Surovtsev, A. And Strok, L., "Theoretical Disquisition on the Static and Dynamic Characteristics of an Adaptive Stepped Hydrostatic Thrust Bearing with a Displacement Compensator," Mathematics, 9, 22, 2021, 2949.
- [10] Singh, U. P., "Mathematical Analysis of Effects of Surface Roughness On Steady Performance of Hydrostatic Thrust Bearings Lubricated with Rabinowitsch Type Fluids", Journal of Applied Fluid Mechanics, 13, 4, 2020, 1339-1347.
- [11] Wada, S. And Hayashi, H., "Hydrodynamic Lubrication of Journal Bearings by Pseudo-Plastic Lubricants: Part 2, Experimental Studies," Bulletin of JSME, 14, 1971, 279-286.
- [12] Wu, Z. And Dareing, D. W., "Non-Newtonian Effects of Powder-Lubricant Slurries in Hydrostatic and Squeeze-Film Bearings," Tribology Transactions, 37, 4, 1994, 836-842.
- [13] Boucherit, H., Lahmar, M., Bou-Saïd, B. And Tichy,

- J., "Comparison of Non-Newtonian Constitutive Laws in Hydrodynamic Lubrication," Tribology Letters, 40,1, 2010, 49-57.
- [14] Esfe, M. H. And Rostamian, H., "Non-Newtonian Power-Law Behavior of Tio2/SAE 50 Nano-Lubricant: An Experimental Report and New Correlation," Journal of Molecular Liquids, 232, 2017, 219-225.
- [15] Ge, Q., Li, Z., Wang, Z., Kowsari, K., Zhang, W., He, X., Zhou, J. And Fang, N.X., "Projection Micro Stereolithography Based 3D Printing and Its Applications," International Journal of Extreme Manufacturing, 2, 2, 2020, 1-19.
- [16] Macaulay, G. D., Senin, N., Giusca, C. L. And Leach, R. K., "Study of Manufacturing and Measurement Reproducibility on a Laser Textured Structured Surface," Measurement, 94, 2016, 942-948.
- [17] Costa, H. And Hutchings I., M., "Some Innovative Surface Texturing Techniques for Tribological Purposes. Proceedings of The Institution of Mechanical Engineers, Part J: Journal of Engineering Tribology, 229, 2015, 429-448.
- [18] Gachot, C., Rosenkranz, A., Hsu, S. M. And Costa, H. L., "A Critical Assessment of Surface Texturing for Friction and Wear Improvement," Wear, 372, 2017, 21-41.
- [19] Singh, A. K., Kumar, V., Singh, S. J. And Sharma, S. C., "Performance of hybrid thrust bearing textured surface operating with electro-rheological lubricant," Proceedings of the Institution of Mechanical Engineers, Part J: Journal of Engineering Tribology, 237,4, 2023, 911-925.
- [20] Wang, J., Zhao, J., Zhang, Y., Wang, D., Li, Y. And Song, Y., "Analysis of The Influence of Wettability On Permeability in Hydrate-Bearing Porous Media Using Pore Network Models Combined with Computed Tomography," Journal of Natural Gas Science and Engineering, 26, 2015, 1372-1379.
- [21] Chawla, M. And Bhardwaj, R., "Surface Roughness Effect on Couple Stress Fluid Lubricated Porous Pivoted Slider Bearings," Journal of Information and Optimization Sciences, 37, 1, 2016, 3-22.
- [22] Kashinath, B. And Nagangouda, H. B., "MHD Effect On Porous Wide Composite Slider Bearing Lubricated with a Couple Stress Fluids," Tribology Online, 10, 1, 2015, 11-20.
- [23] Boubendir, S., Larbi, S. And Bennacer, R., "Numerical Study of the Thermo-Hydrodynamic Lubrication Phenomena in Porous Journal Bearings," Tribology International, 44, 1, 2011, 1-8.
- [24] Nabhani, M., Khlifi, M.E. And Bou-Saïd, B., "Combined Non-Newtonian and Viscous Shear Effects On Porous Squeeze Film Behaviour," Tribology Transactions, 55, 4, 2012, 491-502.
- [25] Patir, N. And Cheng, H. S., "An Average Flow Model for Determining Effects of Three-Dimensional

- Roughness On Partial Hydrodynamic Lubrication," Journal of Lubrication Technology, 101, 2, 1978, 220-229
- [26] Nabhani, M. And El Khlifi, M., "Non-Newtonian Inertial Magnetohydrodynamic Porous Squeeze Film
- Lubrication Between Circular Discs," Tribology International, 94, 2016, 373-382.
- Biradar, T. V., "Squeeze Film Lubrication Between [27] Porous Parallel Stepped Plates with Couple Stress Fluids," Tribology Online, 8, 5, 2013, 278-284.

Nomenclature

- Area of recess; (πR_o^2) , mm^2 A_h
- Area of recess; mm^{2} ; $(\frac{A_b}{A_n} = 4)$ A_n
- Damping coefficient of fluid film, N.s/m; $\left(\bar{C} = \frac{Ch_0^3}{R_0^4 u}\right)$ \mathcal{C}
- Fluid film reaction, N; $\overline{W} = \left(\frac{W}{n_c R_c^2}\right)$ W
- Film thickness at any arbitrary point, mm; $(\bar{h} = h/h_0)$ h
- Runner squeeze/normal velocity, m/s; $(\bar{h} = \frac{\partial \bar{h}}{\partial \bar{t}})$ h
- Nominal film thickness, mm h_{o}
- Stiffness parameter, N/mm; $\left(\overline{K} = \frac{h_o}{p_s R_o^2} K\right)$ K
- Lubricant pressure, MPa; $(\bar{p} = \frac{p}{n_c})$ p
- Fluid pressure in recess, MPa; $(\bar{p}_r = \frac{p_r}{n_s})$ p_r
- R_{si} Inner radius of recess, mm
- Outer radius of recess, mm R_{so}
- Radius of thrust pad, mm R_o
- Radius of any point on thrust pad, mm; $\left(\bar{r} = \frac{r}{R_0}\right)$ r
- Cartesian coordinates, mm; $\left(\bar{x} = \frac{x}{R_o}; \bar{y} = \frac{z}{R_o}; \bar{z} = \frac{y}{h_o}\right)$ Permeability of porous facing, m^2 x, y, z
- ψ